Applied Surface Science 387 (2016) 882–893

Contents lists available at ScienceDirect

Applied Surface Science

journal homepage: www.elsevier.com/locate/apsusc

Enhanced visible light photocatalytic performance of polyaniline modified mesoporous single crystal TiO_2 microsphere

Yaocheng Deng[a,b], Lin Tang[a,b,*], Guangming Zeng[a,b,*], Haoran Dong[a,b], Ming Yan[a,b], Jingjing Wang[a,b], Wei Hu[c], Jiajia Wang[a,b], Yaoyu Zhou[a,b], Jing Tang[a,b]

[a] College of Environmental Science and Engineering, Hunan University, Changsha, 410082, China
[b] Key Laboratory of Environmental Biology and Pollution Control, Hunan University, Ministry of Education, Changsha 410082, China
[c] College of Physics and Microelectronics Science, Hunan University, Changsha, 410082, China

ARTICLE INFO

Article history:
Received 11 June 2016
Received in revised form 1 July 2016
Accepted 3 July 2016
Available online 5 July 2016

Keywords:
Mesoporous single crystal
Visible light irradiation
Photocatalytic activity
Polyaniline

ABSTRACT

Polyaniline (PANI) modified mesoporous single crystal TiO_2 microsphere (PANI/MS-TiO_2) with excellent photocatalytic activity was successfully prepared by a simple method of solution evaporation and chemisorption. The X-ray diffraction characterization demonstrated that the whole MS-TiO_2 kept the crystal type of anatase. The nitrogen adsorption-desorption characterization coupled with scanning electron microscopy indicated that the MS-TiO_2 possessed a unique mesoporous structure with high specific surface area, which resulted in the increased load of PANI on the surface of MS-TiO_2 and multiple light reflection in the photocatalyst. The UV–vis diffuse reflectance spectra confirmed that PANI/MS-TiO_2 presented more absorption ability in the visible light range than that of the pristine MS-TiO_2. The transient photocurrent responses and electrochemical impedance spectroscopy (EIS) indicated the high photo responses and fast photogenerated charge separation efficiency of PANI/MS-TiO_2. The photocatalytic activity of the PANI/MS-TiO_2 was evaluated by the photodegradation of RhB and MB under visible light irradiation. MS-TiO_2 photocatalyst with different molar ration of PANI had been prepared, and the results showed that the optimal photocatalyst (PANI/MS-TiO_2 (1:40)) exhibited the highest photocatalytic efficiency which is nearly three times as great as that of pristine MS-TiO_2 for the degradation of the RhB and MB under visible light irradiation. The remarkable performance of the PANI/MS-TiO_2 under visible light was attributed to its mesoporous single crystal structure with large surface, conductivity, as well as the synergistic effect between PANI and MS-TiO_2.

1. Introduction

In recent decades, many researchers have been engaged in finding and developing a more effective method for the treatment of organic dye wastewater or other environmental pollutants. Photocatalysis, based on clean solar energy and semiconductor as the photocatalyst, has become a very promising strategy with low cost, high activity and no secondary pollution in the environment [1–7]. TiO_2 has been proved to be among the most efficient photocatalysts due to its extraordinary photostability, good mechanical flexibility, high photocatalytic activity and non-toxicity [8,9]. However, because of the relative wide band gap (~3.2 eV), TiO_2 can only utilize the ultraviolet light, which just occupied 4% of the whole solar light, so the wide use of TiO_2 is limited severely. Therefore, in order to change the unfavorable situation and improve the solar light utilization and photocatalytic efficiency of TiO_2, much efforts shifting the photoresponse area of TiO_2 from ultraviolet to the visible light range have been made, such as doping with noble metal [10,11], metal ion [12], non-metal ion [13] and coupling with relative narrow band-gap semiconductors [14–18]. Though the modification mentioned above can partly enhance the photocatalytic performance of TiO_2, there still exist some unresolved problems. For example, decorating with other materials will bring a threat to the thermal stability for the whole photocatalytic system and the increase of recombination probability between photoelectron and carrier.

Recently, conducting polymers, such as polypyrrole, polythiophene, and polyaniline (PANI) have been widely studied as excellent sensitizers to improve the visible light utilization and photocatalytic efficiency of TiO_2 photocatalysts [19–21]. The improvement of the photocatalytic performance of TiO_2 by con-

* Corresponding authors at: College of Environmental Science and Engineering, Hunan University, Changsha, 410082, China.
E-mail addresses: tanglin@hnu.edu.cn (L. Tang), zgming@hnu.edu.cn (G. Zeng).

http://dx.doi.org/10.1016/j.apsusc.2016.07.026
0169-4332/

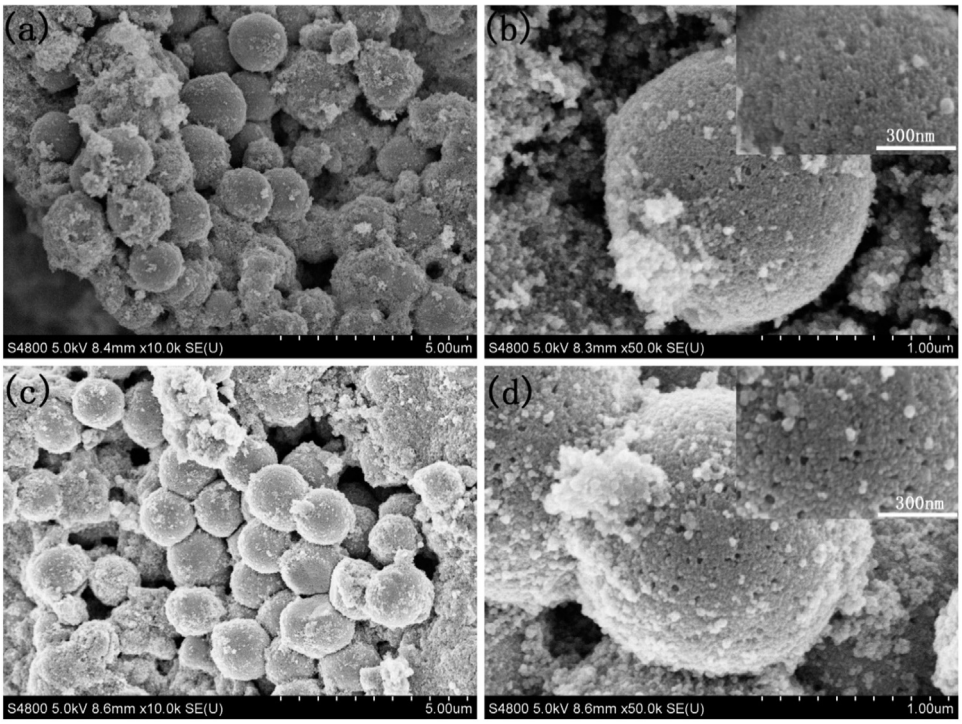

Fig. 1. SEM image of (a and b) MS-TiO_2 and (c and d) PANI/MS-TiO_2 (1:40).

ducting polymers decoration is mainly due to the increased visible light absorption property and rapid charge separation as a result of the synergistic action between the conducting polymers and TiO_2. Zhang et al. prepared PANI/TiO_2 composites via in situ polymerization and chemisorption method [22]. The prepared PANI/TiO_2 photocatalyst presented remarkably higher photocatalytic performance than that of untreated TiO_2 particles on degradation of RhB and MB under UV and visible light irradiation. Salem and coworkers also found that the photocatalytic efficiency of TiO_2 had been improved when modified by PANI [23]. However, the photocatalytic activity of these PANI modified TiO_2 nanoparticles were inhibited by the low visible light utilization efficiency. Hence, it is necessary to promote the visible light utilization efficiency of the PANI modified TiO_2 nanoparticle hybrid photocatalyst for higher photocatalytic activity under visible light irradiation.

Large surface area is a key point to promote the photocatalytic efficiency of modified TiO_2 hybrid photocatalyst in the visible light region, which can increase the load amount of the sensitizer, thus improving the visible light absorption in return. In view of that reason, mesoporous semiconductors and materials have attracted great attention due to their large surface structure for environmental and energy applications [24–29]. However, most of the mesoporous materials own polycrystalline or amorphous structure, which are not conducive to the transportation of the photogenerated electron and increase the recombination efficiency. Hence, the photocatalytic activity based on these polycrystalline or amorphous semiconductor was greatly restricted. To solve this problem, Liao and coworker carried out the research on core-shell mesoporous TiO_2 modified by PANI. The specific core-shell mesoporous structure can provide large surface area, and the single crystal type can bring about excellent charge separation efficiency. When sensitized by PANI, the hybrid composites exhibited remarkably photocatalytic activity for the degradation of RhB and phenol under visible light irradiation [30]. Very recently, Liu et al. successfully developed a type of dye sensitized solar cell based on mesoporous single crystal TiO_2 microsphere (MS-TiO_2) and obtained great energy conversion efficiency compared with the conventional TiO_2 nanoparticles based solar cells, which is mainly contributed to the high surface area, efficient charge transfer and separation properties of MS-TiO_2 [31]. Due to the great performance of MS-TiO_2 exhibited in the prepared new type solar cell in Liu's study, we have reasons to expect that MS-TiO_2 may be a good matrix for conducting polymer decoration for its large surface area and unique mesoporous single crystal structure.

In this work, we developed polyaniline (PANI) modified mesoporous single crystal TiO_2 microsphere (PANI/MS-TiO_2) by a simple method of solution evaporation and chemisorption. The synergistic action between PANI and the special TiO_2 microsphere coupled with mesoporous single crystal structure could promote the separation efficiency of photogenerated electron and hole. Its good visible light response is expected. Meanwhile, the effective charge separation property and efficient visible light utilization could improve the photocatalytic activity of the PANI/MS-TiO_2 hybrid composite remarkably under visible light irradiation. To evaluate the photocatalytic activity of the as-prepared PANI decorated MS-TiO_2, rhodamine B (RhB) and methylene blue (MB) were used as objective contaminants for photocatalytic degradation reactions under visible light irradiation ($\lambda > 400$ nm).

2. Experimental

2.1. Materials

Titanium butoxide (TBOT, ≥99%) were obtained from Aladdin Industrial Corporation, Pluronic copolymer F127 was purchased from sigma-Aldrich Corporation, Aniline (≥99.5%) and ammonium persulfate ($(NH_4)_2S_2O_8$, ≥98%) were purchased from Tianjin Kemiou Chemical Reagent Co., Ltd. Tetrahydrofuran (THF), Acetic Acid (HOAc, ≥99.5%), Hydrochloric acid (HCl, 36%) and all the other chemical agent were obtained from Sinopharm Chemical Reagent Co., Ltd. All chemical agents were used without further purification.

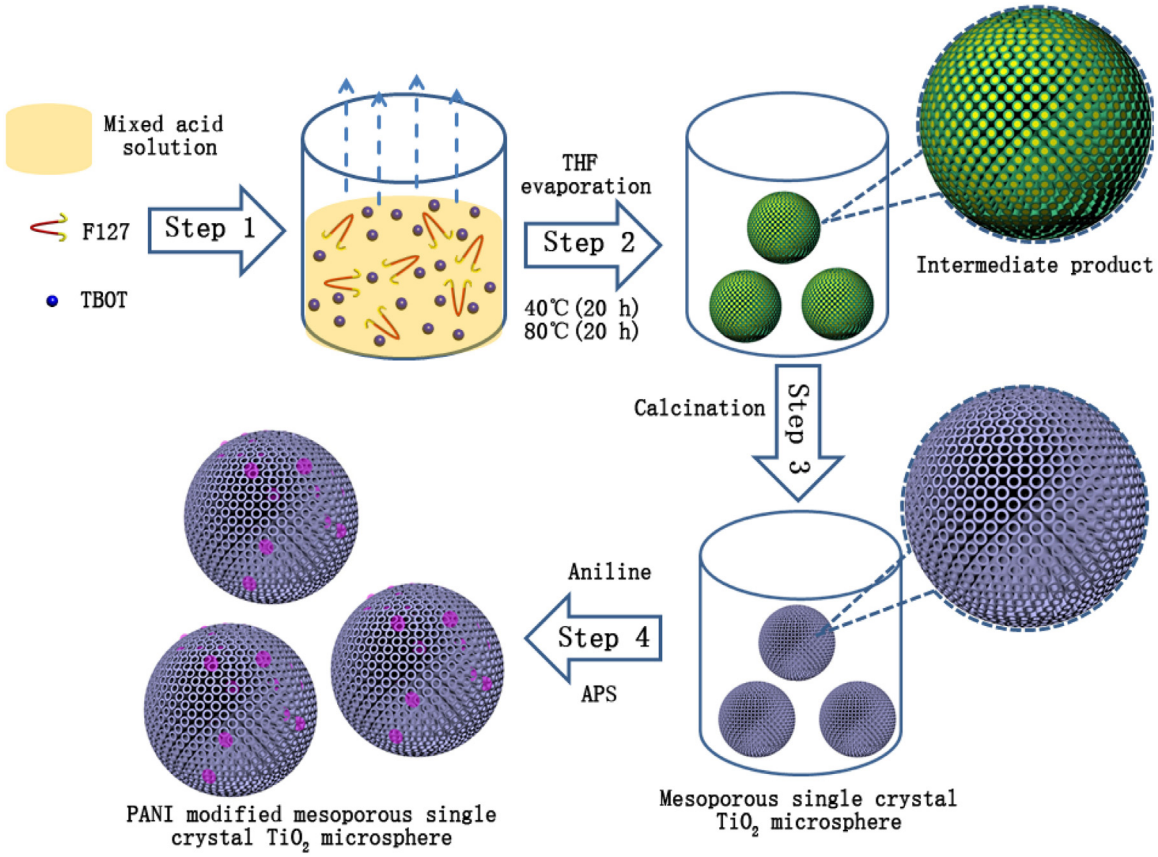

Scheme 1. The formation process of the mesoporous single crystal TiO_2 microsphere photocatalyst.

2.2. Preparation of MS-TiO_2

Mesoporous single crystal TiO_2 microspheres (MS-TiO_2) were synthesized according to a reported method with some modification [31]. In a typical synthesis, 1.6 g of F127 was dissolved in 30 ml THF. After stirring for 10 min, 2.4 g of HCl and 2.4 g of HOAc were added to the mixture. Then the mixture was stirred for another 30 min to obtain a clear and transparent solution. Subsequently, 3.4 g of TBOT was added to the mixture drop by drop and keep vigorous stirring for next 30 min to obtained clear golden yellow solution. Next, 0.2 g H_2O was added to the mixture and kept stirring for another 10 min. Then the golden yellow solution was transferred to volumetric flasks (30 mm*50 mm) and kept at 40 °C for 20 h in an electric oven to evaporate THF solvent. Followed by drying at 80 °C for 20 h to remove the THF solvent completely, white solid intermediate product was formed. Finally, the MS-TiO_2 can be obtained by calculating the white solid product in tube furnace at 350 °C for 2 h under N_2 flow and in muffle furnace at 400 °C for 3 h in air, successively.

2.3. Preparation of PANI/MS-TiO_2

Polyaniline modified MS-TiO_2 were prepared by a method of chemical oxidative polymerization of aniline in the presence of MS-TiO_2 microspheres. First of all, 0.5 g of prepared MS-TiO_2 was dispersed into 50 ml of 1 M HCl aqueous solutions in a three-neck flask and sonicated for 30 min to form a uniform suspension. After that, certain amount of aniline was added into the above mixture under vigorously mechanical stirring in the ice-water bath and kept for 60 min. Secondly, ammonium persulfate (APS) was dissolved in 20 ml of 1 M HCl aqueous solution with the molar ratio of aniline to APS (1:1) which was added dropwise to the above flask via a burette. Then the mixed solution was allowed to stir for 4 h to polymerize efficiently. Finally, when the reaction was finished, the polyaniline modified MS-TiO_2 was filtered and washed with large amount of ethanol and deionized water. Then the synthesized composites were dried at 60 °C for 12 h to obtain a constant mass. In the experiment mentioned above, to prepare a series of PANI modified MS-TiO_2 samples, different initial molar ratios of aniline to MS-TiO_2 (from 1:20 to 1:80) were used, and the samples were labeled as PANI/MS-TiO_2 (1:20), PANI/MS-TiO_2 (1:40), PANI/MS-TiO_2 (1:60) and PANI/MS-TiO_2 (1:80), respectively. To confirm and ensure the effect of PANI in this study, the original MS-TiO_2 was treated in the same process without the addition of aniline and APS. Additionally, to further study the function of the mesoporous single crystal microsphere structure of TiO_2 in the photocatalytic system, the MS-TiO_2 was destroyed by grounding and used as the body materials for PANI coating, which are labeled as PANI/broken MS-TiO_2. The whole preparation process of the PANI/MS-TiO_2 was presented briefly and clearly in Scheme 1.

2.4. Characterization

The morphology of the prepared samples was characterized by Field-emission scanning electron microscopy (FE-SEM) (Hitachi S-4800, Japan) with an accelerating voltage of 5 kV. Transmission electron microscopy (TEM, Tecnai G2 F20 S-TWIN) and high-resolution transmission electron microcopy (HR-TEM) with an accelerating voltage of 200 kV was used to characterize the detailed structure of the samples. The crystal structure of the prepared samples was investigated by using an X-ray diffractometer (XRD) (Bruker D8 Advances). The optical property of the prepared samples was measured through ultraviolet visible diffuse reflectance spectra (DRS) by a UV–vis spectrophotometer (Cary 300,

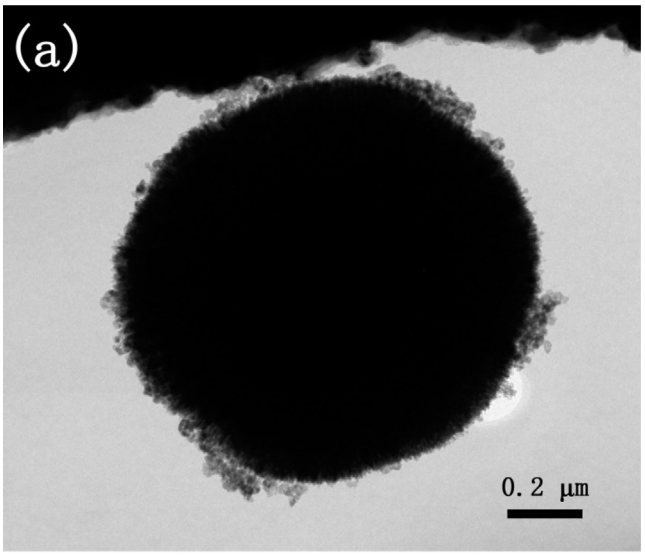

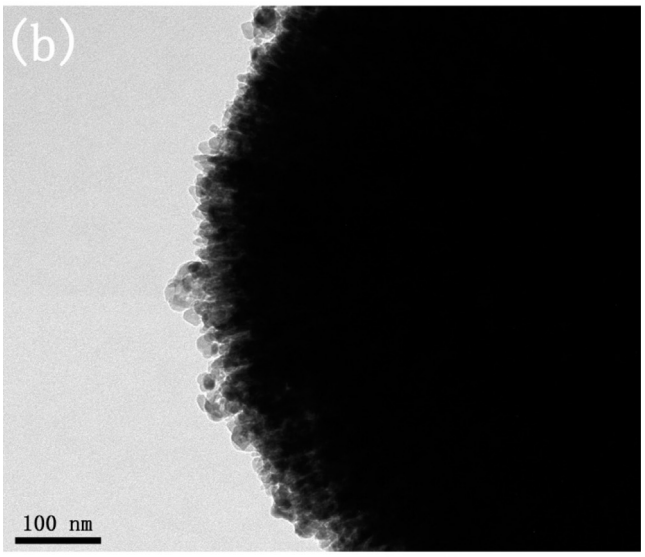

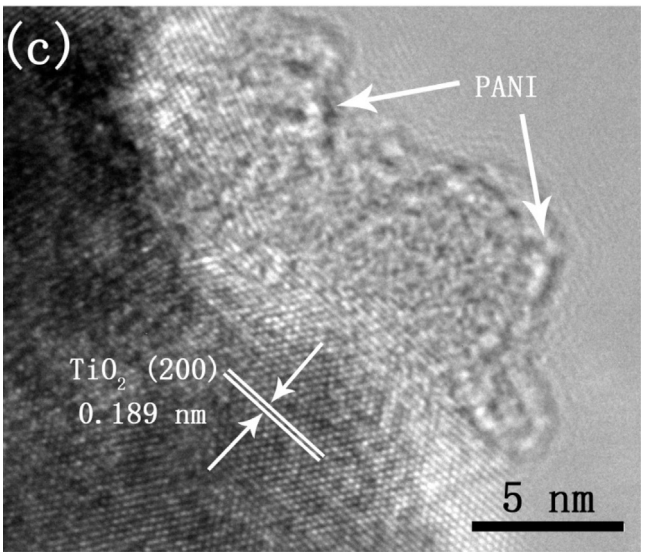

Fig. 2. (a) Low and (b) high magnification TEM images and (c) HR-TEM image of PANI/MS-TiO_2 (1:40).

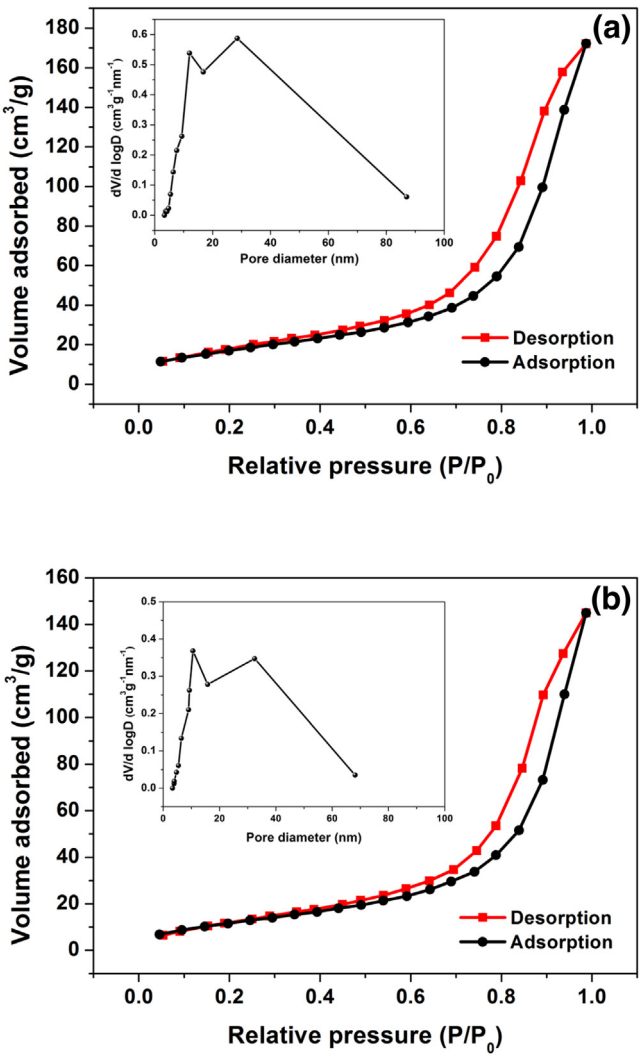

Fig. 3. Nitrogen adsorption-desorption isotherms and the corresponding pore size distribution plot of (a) MS-TiO_2 and (b) PANI/MS-TiO_2 (1:40).

USA), and their bonding structure information were measured by Fourier transformed infrared spectroscopy (FT-IR, type) with KBr as the reference sample. The specific surface areas of the samples were characterized via a nitrogen adsorption-desorption and Brunauer-Emmett-Teller (BET) method by a surface area analyzer (Micromeritics ASAP 2020).

2.5. Photocatalytic experimental

The photocatalytic activities of the samples were evaluated by the degradation of rhodamine B (RhB) and methylene blue (MB) in aqueous solution. Typically, 50 ml of RhB or MB aqueous solution with concentration of 10 mg/l was mixed with 50 mg PANI/MS-TiO_2 catalysts. A 300 W xenon lamp (Beijing Perfectlight Technology Co. Lt, PLS-SXE 300C) equipped with a UV-cut filter ($\lambda > 400$ nm) was used as the visible light source. Before turning on the lamp, the mixture was stirred in the dark for 60 min to reach adsorption-desorption equilibrium between the photocatalyst and RhB/MB. The photocatalytic activity experiments were conducted in a 100 ml quartz reaction vessel and the irradiation distance between the lamp and the sample was 20 cm. At certain time intervals, 2 ml aliquots were collected and sampled, then centrifuged at 10000 rpm for 10 min to remove the photocatalyst. The real-time concentration of RhB or MB was determined by recording

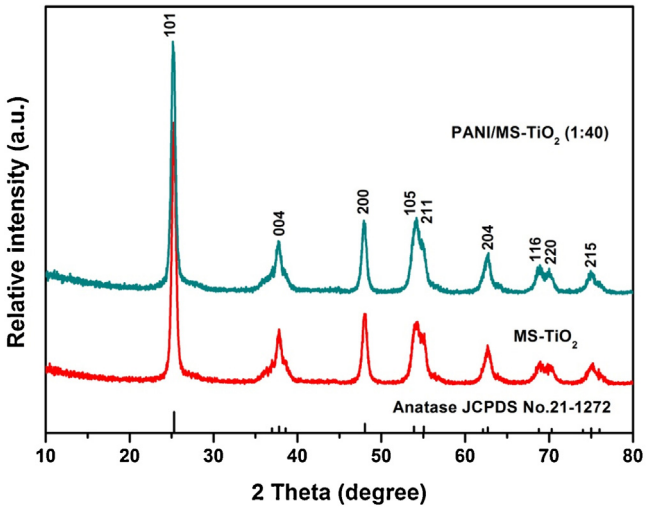

Fig. 4. XRD patterns of MS-TiO_2 and PANI/MS-TiO_2 (1:40).

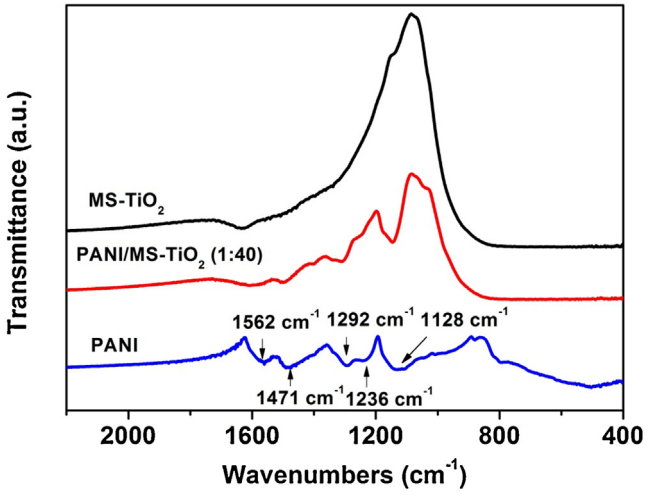

Fig. 5. FT-IR spectrum of PANI, MS-TiO_2 and PANI/MS-TiO_2 (1:40).

the maximum UV–vis absorption using UV–vis spectrophotometer (UV-2550, Shimadzu, Japan).

2.6. Photoelectrochemical measurement

To study the photoelectrochemical properties of prepared samples, the working electrodes were prepared as follows: 10 mg of the photocatalyst was suspended in 1 ml 0.5% Nafion solution to make slurry. Then, Then 100 μl of the slurry dropped onto a 1 cm × 2 cm FTO slice with an effective working area of 1 cm^2. All the photoelectrochemical measurements were measured on a CHI 660D electrochemical analyzer with a standard three-electrode system using the prepared samples coated on FTO glass as the working electrode, a Pt electrode as the counter electrode, and Ag/AgCl electrode as a reference electrode. A 300 W Xe arc lamp served as a light source. The photocurrent and electrochemical impedance spectroscopy (EIS) was performed in 0.2 Na_2SO_4 aqueous solution. The EIS frequency ranged from 0.01 HZ to 10^5 HZ with an alternating current amplitude of 10 mV.

2.7. Active species trapping experiments and recycle experiments

In order to detect the role of the active species in the photocatalytic process, isopropanol (IPA), triethanolamine (TEOA) or benzoquinone (BQ) were added to the photocatalytic system to investigate the function of hydroxyl radical (•OH), hole (h^+) and superoxide radical ($•O_2^-$), respectively. In the recycle experiments, the photocatalyst were collected and washed with deionized water for several times, and dried at 60 °C for 12 h. Due to the inevitable weight loss of the photocatalyst in the process of experiments, some fresh catalysts was added to ensure the accuracy of the results of the experiments. Then the dried photocatalyst couple with little fresh catalysts was used in the next photocatalytic experiments.

3. Results and discussion

3.1. Morphology of MS-TiO_2 and PANI/MS-TiO_2

The scanning electron microscopy (SEM) images of the prepared MS-TiO_2 are shown in Fig. 1a and b. It can be seen that the prepared samples composed of uniform microspheres with a diameter of ~800 nm. The surface of these microspheres was not smooth but with a lot of porous, which indicated the prepared samples owned a sphere and mesoporous structure as well. After the modification process of PANI was finished, the morphology of PANI/MS-TiO_2 was presented in Fig. 1c and d. It is clear to notice that there were not any obvious changes compared with that of origin MS-TiO_2, which indicates that the PANI layer coated on the surface of the MS-TiO_2 was very thin. To investigate the detailed morphology of the prepared PANI/MS-TiO_2 samples, transmission electron microscopy (TEM) and high-resolution transmission electron microscopy (HR-TEM) were measured. As shown in Fig. 2a, it is clear to see that the prepared samples kept the morphology of microsphere. In Fig. 2b, on the edge of the microsphere, there existed a lot of closed-packed cylindrical and these cylindrical were arranged radially from the center to the surface. The typical HR-TEM image of PANI/MS-TiO_2 (1:40) are shown in Fig. 2c, it can be seen that in the crystalline part, the lattice distance was 0.189 nm, which belonged to the 200 crystalline plane of anatase TiO_2. But in the edge and surface of the TiO_2, there existed a region of noncrystal structure layer, which should be the layer of PANI. Because the prepared PANI molecules tended to aggregate on the surface of TiO_2, and other research group obtained the similar phenomenon [22,32].

3.2. Porous structure and distribution determination

To measure and analysis the specific surface areas and pore size distribution of the prepared MS-TiO_2 and PANI/MS-TiO_2, nitrogen gas absorption-desorption isotherm curves and relative Barrett-Joyner-Halenda method were conducted. As shown in Fig. 3a, it is clearly to see that the prepared samples owned a mesoporous structure, and the calculated specific surface area and pore volume were as high as 95.3 m^2/g and 0.394 cm^3/g, respectively. From the inset picture in Fig. 3a, it can be clearly seen that there exited two sets of pores. The center of the primary pore size was located on 12 nm, and the secondary pore size was focused at 30 nm. Owing to the high specific surface area of MS-TiO_2, a large number of PANI molecules could be absorbed on to the surface of MS-TiO_2, which enhanced the visible light absorption ability of the PANI/TiO_2 greatly. To make comparison, the nitrogen adsorption-desorption isotherms and relative Barrett-Joyner-Halenda curves of PANI/TiO_2 (1:40) were also provided (shown in Fig. 3b). The PANI/MS-TiO_2 (1:40) still kept the mesoporous structure, and the pore size distribution was also similar to pristine MS-TiO_2. The specific surface area and pore volume of the PANI/MS-TiO_2 (1:40) were measured as 82.7 m^2/g and 0.271 m^3/g, respectively. Though the specific surface area and pore volume of the PANI/MS-TiO_2 (1:40) were slightly lower than that of MS-TiO_2 due to the cover of PANI molecules, it was still able to provide lots of active sites for the interfacial reac-

tion process and to promote the photocatalytic performance of the whole photodegradation system.

3.3. Crystal structure of MS-TiO_2 and PANI/MS-TiO_2

The X-ray diffraction patterns (XRD) was used to determine the crystal structure of the MS-TiO_2 and PANI/MS-TiO_2 (1:40). Just as the curves shown in Fig. 4, both MS-TiO_2 and PANI/MS-TiO_2 (1:40) presented anatase TiO_2 crystal structure and owned the dominant lattice plane of 101 lattice plane (JCPDS No.21-1272). And meanwhile, it should be noted that the peak positions and shapes of PANI/MS-TiO_2 (1:40) in the patterns did not show clearly difference from that of MS-TiO_2, indicating that the PANI decoration process did not influence the lattice structure and crystal type of pristine MS-TiO_2, which would ultimately bring about great benefits to the photocatalytic activity and the photodegradation performance of the prepared composite photocatalyst. [20,30,33]

3.4. FT-IR analysis

The Fourier Transform Infrared Spectroscopy (FT-IR spectroscopy) of MS-TiO_2 and PANI/MS-TiO_2 (1:40) was used to characterize the interaction between the MS-TiO_2 and PANI, and the results were presented in Fig. 5. For comparison, the FT-IR of pure PANI was also provided. It is clear to see that the characteristic absorption bands of PANI were mainly located at 1128 cm^{-1}, 1236 cm^{-1}, 1292 cm^{-1}, 1471 cm^{-1} and 1562 cm^{-1}. The peak at 1128 cm^{-1} is related to the plane bending vibration of C—H. The peaks at 1236 cm^{-1} and 1292 cm^{-1} are ascribed to C—N stretching mode of benzenoid unit [30,32]. The peak at 1471 cm^{-1} can be attributed to C=C stretching mode for benzenoid unit, and the peak at 1562 cm^{-1} can be referred to the C=C stretching mode for the quinonoid unit [23,34]. Furthermore, all characteristic absorption bands of PANI appeared in PANI/MS-TiO_2, implying the existence of PANI in PANI/MS-TiO_2 (1:40).

3.5. XPS analysis

As shown in Fig. 6, the X-ray photoelectron spectroscopy (XPS) was provided to determine the information about the surface electronic state and functional groups involved in PANI/MS-TiO_2 nanocomposites. In Fig. 6a, the XPS survey spectrum demonstrated that there exist four elements in the hybrid photocatalyst, Ti, O, C, and N. The XPS spectrum of Ti is shown in Fig. 6b. There exist two main peaks at 458.28 and 464.22 eV, which are corresponding to the Ti $2p_{2/3}$ and Ti $2p_{1/2}$, respectively [31]. The XPS spectrum of O is shown in Fig. 6c. The peak at 529.63 eV is assigned to Ti—O—Ti, and another peak at 531.42 eV is attributed to the H bonding of between PANI and TiO_2 [35]. Fig. 6d presents the C 1s spectrum. It can be seen that there exist three banding energies located at 284.17, 286.19, and 288.42 eV. And these three binding energies are referred to different forms of carbon. The peak at 284.17 eV is related to CC and C=C, while the peak at 286.19 and 288.42 eV are ascribed to C—O—Ti and C=O, respectively [36]. Fig. 6f presents the N 1 s XPS spectrum. It is clearly to see that there exist four forms of N. The peaks at 401.55 eV and 398.74 eV are related to pyrrolic N and pyridinic N, respectively. The peak at 400.74 eV could be contributed to the interaction between protons and N^+ due to the acid doping, and the peak at 399.86 eV resulted from the interaction between the metal ions and nitrogen (M—N) [37]. According to the XPS analysis mentioned above, the existence of CO—Ti, M—N bonds in the PANI/MS-TiO_2 hybrid photocatalyst further demonstrated the existence of PANI on MS-TiO_2 and the interaction happened between PANI and mesoporous single crystal TiO_2 microsphere.

3.6. UV–vis diffuse reflectance spectra

The optical absorption properties of the as-prepared MS-TiO_2 and PANI/MS-TiO_2 (1:40) samples were measured using UV–vis diffuse reflectance spectra. As shown in Fig. 7, it is obvious that the absorption range of MS-TiO_2 was just limited at UV light and exhibited primary absorption edge of around 420 nm. However, PANI/MS-TiO_2 (1:40) presented a high absorption around the whole range of visible light, which indicated the PANI coated on the MS-TiO_2 improved the absorption ability greatly and broadened the absorption range of MS-TiO_2 to visible light. This promotion can be attributed to the unique mesoporous and microsphere structure of MS-TiO_2. On the one hand, mesoporous structure of MS-TiO_2 provided large specific surface areas, which increased the loading amount of PANI molecules, and enhanced the absorption ability of the hybrid photocatalyst in visible light. Meanwhile, the mesoporous and rough surface of PANI/MS-TiO_2 showed great advantages for the photons to enter into photocatalyst than the smooth one. On the other hand, due to the existence of the pores, when the visible light propagated in the photocatalyst, more light reflection and scatter would happen in the interior cavity of PANI/MS-TiO_2 (1:40), which increased the optical path length in the composite, so as to present great enhancement in the absorption of visible light. Therefore, these factors mentioned above combined resulted in the enhanced photocatalytic activity and photodegradation ability of the hybrid photocatalyst.

3.7. Transient photocurrent responses (I-t) and electrochemical impedance spectra (EIS)

Transient photocurrent under visible light irradiation and electrochemical impedance spectra (EIS) was measured to further understand the photogenerated charge separation and electron transfer performance of the prepared samples. As shown in Fig. 8a, both of MS-TiO_2 and PANI/MS-TiO_2 (1:40) presented photocurrent when under visible light irradiation, but pure MS-TiO_2 presented very low photocurrent, which means the low visible light response. And meanwhile, the PANI/MS-TiO_2 (1:40) sample exhibits high photocurrent responses than that of MS-TiO_2, which indicating that PANI/MS-TiO_2 (1:40) performed better visible light response due to the coating of PANI molecules. Electrochemical impedance spectroscopy (EIS) was also carried out to provide additional evidence for the improved charge separation in the prepared samples, and the semicircular of the Nyquist plots were referred to the resistance of the electrodes. Just as shown in Fig. 8b, once the MS-TiO_2 was coated with PANI molecular, its EIS semicircular experienced a dramatically decrease, which indicating that the coating of PANI could facilitate the interfacial charge transfer. According to the transient Photocurrent responses and electrochemical impedance spectra analysis, we can see that the prepared PANI/MS-TiO_2 shown great visible light response ability and low resistance to inhibit the transportation of photogenerated charges, which could greatly promote the photocatalytic activity of the prepared PANI/MS-TiO_2 photocatalyst.

3.8. Photocatalytic capability

The photocatalytic activities of the MS-TiO_2 and PANI/MS-TiO_2 were evaluated by the degradation of RhB and MB under visible light irradiation ($\lambda > 400$ nm). Fig. 9 presents the photodegradation of RhB and MB as functions of visible light irradiation time for the MS-TiO_2 and different molar ratio of PANI/MS-TiO_2 catalyst. For comparison, the absence of light irradiation or catalyst was also concluded in this study. As shown in Fig. 9, when the irradiation was turned off or the catalyst was not added, there was no obvious degradation of RhB and MB. While once the MS-TiO_2 or

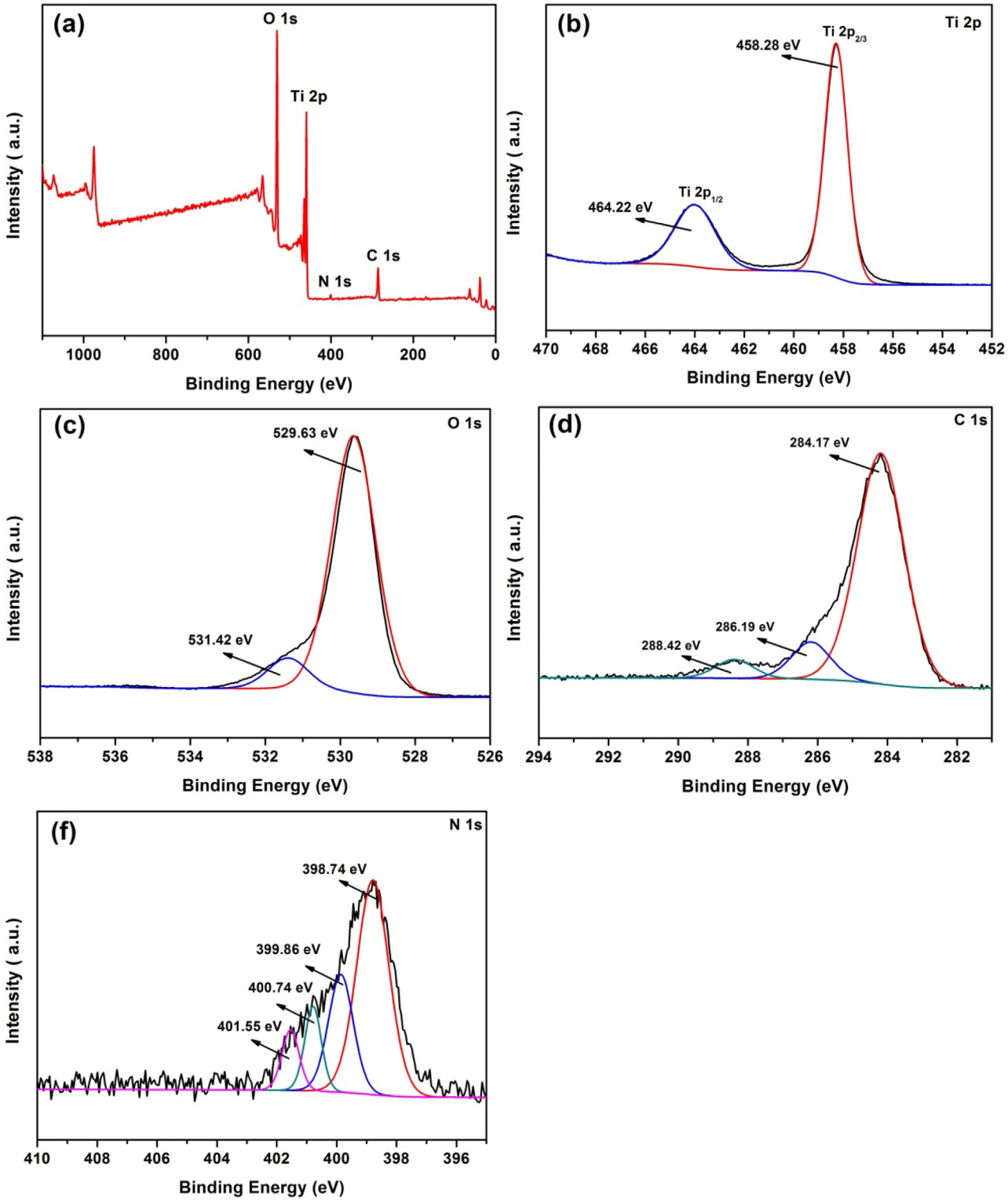

Fig. 6. XPS spectra of the PANI/MS-TiO_2 (1:40) (a) survey spectrum, (b) Ti 2p, (c) O 1s, (d) C 1s, and (d) N 1s.

PANI/MS-TiO_2 was added into the dye solution under the visible irradiation, the photocatalytic activities enhanced greatly, especially for PANI/MS-TiO_2. The results showed that the photocatalytic activity was enhanced gradually with increasing the molar ratio of PANI. When the molar ratio proportion of PANI to MS-TiO_2 got to 1:40, the prepared photocatalyst reached optimal photocatalytic activity that could degrade RhB by 99.8% in 120 min and MB by 99.5% in 150 min. But once the proportion of PANI increased to 1:20, the photocatalytic capability of PANI/MS-TiO_2 decreased to 98.6% of RhB and 98.4% of MB. The reason was that when the molar ratio of PANI to MS-TiO_2 surpassed 1:40, the redundant PANI molecules were easy to gather on the surface of MS-TiO_2, which affected the separation of the photoinduced electron-hole pairs and the transportation of the photogenerated charges. To further demon-

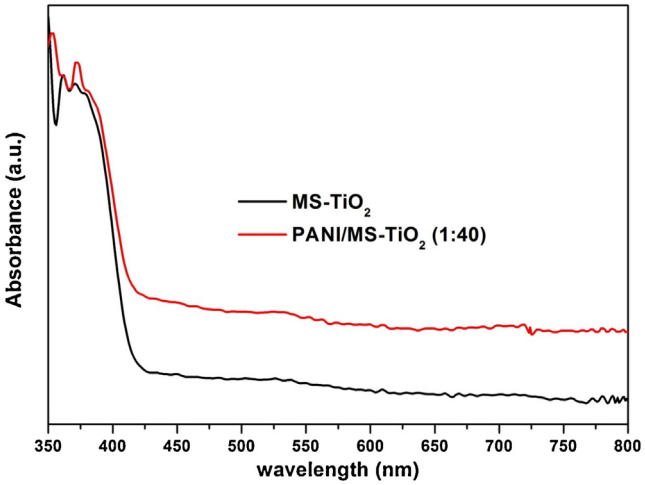

Fig. 7. UV–vis diffuse reflectance spectra of MS-TiO_2 and PANI/MS-TiO_2 (1:40).

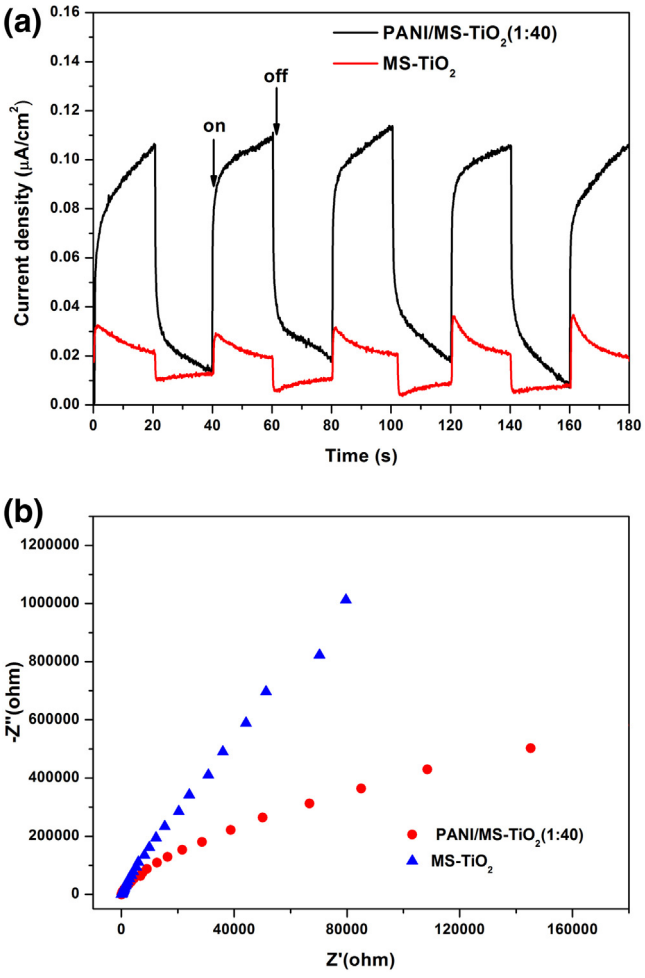

Fig. 8. (a) Transient photocurrent response and (b) Nyquist plots of EIS obtained for MS-TiO_2 and PANI/MS-TiO_2 (1:40).

strated the mesoporous single crystal and microsphere structure of TiO_2 was beneficial for the enhance photocatalytic activity, the PANI/broken MS-TiO_2 (1:40) was also used in this photocatalytic system. Just as shown in Fig. 9, when the structure of MS-TiO_2 was broken, the photodegradation efficiency of RhB and MB were both decreased, which implying that the special structure of MS-TiO_2

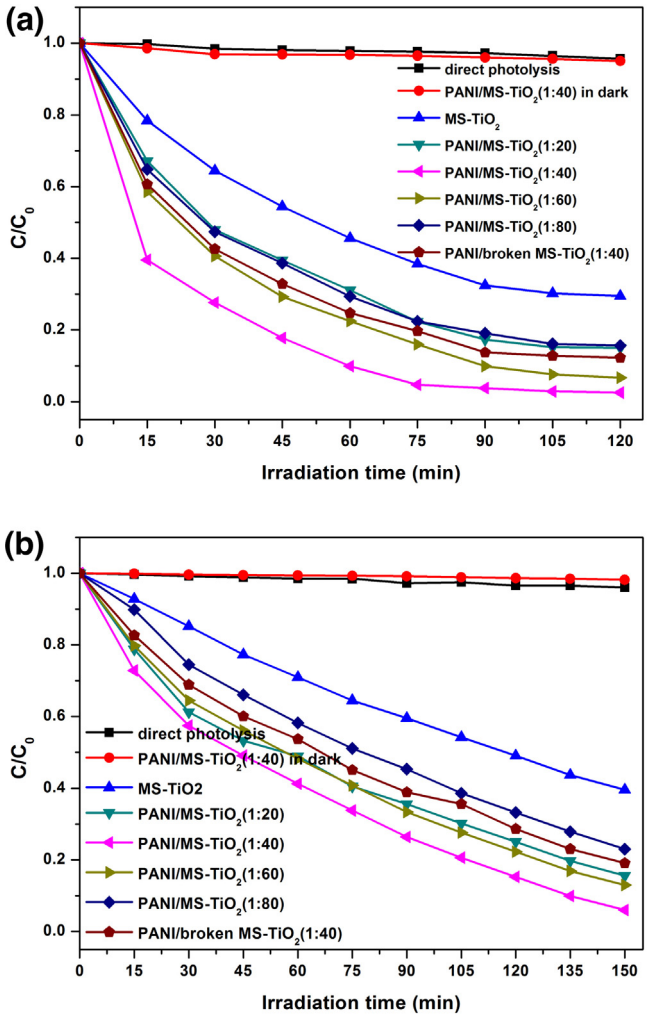

Fig. 9. Photocatalytic degradation of (a) RhB and (b) MB in the presence of different composites under visible-light (λ > 400 nm) irradiation.

played an important role in promoting the photocatalytic reaction process.

Fig. 10 shows the changes of the UV–vis absorption spectra as a function of time during the photocatalytic degradation of RhB and MB over PANI/MS-TiO_2 (1:40) catalyst. As shown in Fig. 10a, b), in the process of adsorption-desorption equilibrium, only the characteristic absorbance peak of RhB (MB) at 554 nm (664 nm) decreased. After 15 min of irradiation, the absorption peak of the RhB aqueous solution showed sharp blue-shifts and broadening, simultaneously. The blue-shift of the absorption peak implied a step by step de-ethylation process during the photodegradation of RhB. This phenomenon was also presented during the process of the degradation of MB. And this phenomenon in this study was also found in other research groups. [38–42]

It is found that the photodegradation of organic pollutants under different catalysts accorded with pseudo-first-order kinetic (Fig. 11). The relative kinetic constants were calculated by the following equation [22,30].

$$\ln(C/C_0) = -kt \quad (1)$$

where C is the concentration of organic pollutants at the time of t, C_0 is the initial concentration of the organic pollutants, and k is the corresponding kinetic constant. As shown in Fig. 11, under the same experiment conditions, the kinetic constant of RhB and MB degradation with PANI/MS-TiO_2 (1:40) presented the highest

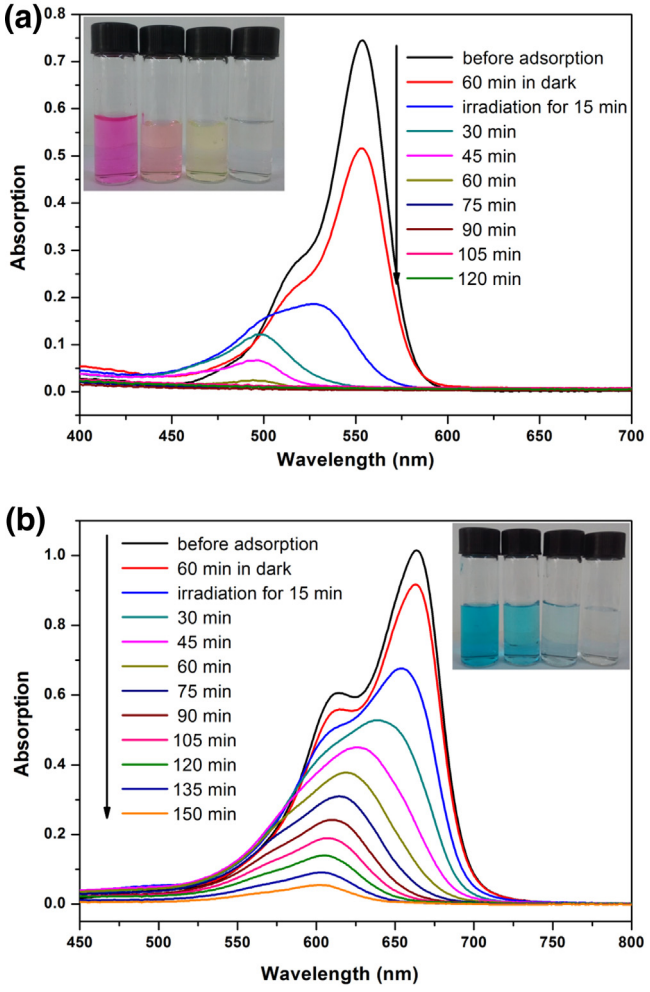

Fig. 10. Time-dependent UV–vis absorption spectra and relative color changes of (a) RhB and (b) MB over different composites.

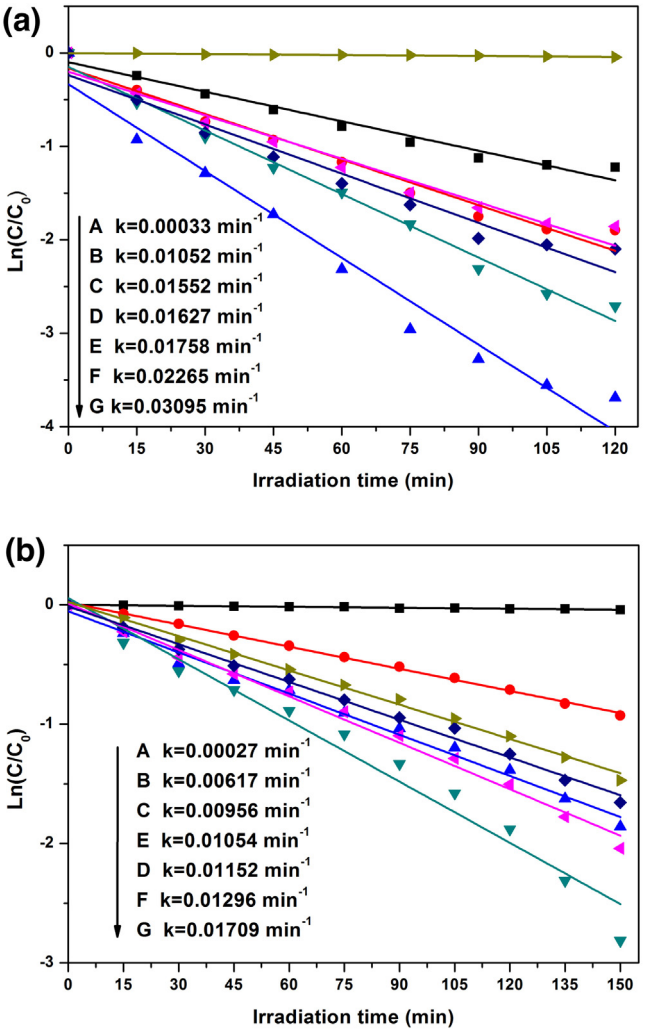

Fig. 11. Plots of degradation of (a) RhB and (b) MB over different PANI/MS-TiO_2 under visible light irradiation: (A) blank; (B) MS-TiO_2; (C) PANI/MS-TiO_2 (1:80); (D) PANI/MS-TiO_2 (1:20); (E) PANI/broken MS-TiO_2 (1:40) (F) PANI/MS-TiO_2 (1:60); (G) PANI/MS-TiO_2 (1:40).

degradation rates, which were 0.03095 min^{-1} and 0.01709 min^{-1}, respectively, which are nearly three times as great as that of the origin MS-TiO_2. The high kinetic constant means the advantages of the unique structure in the PANI/MS-TiO_2 photocatalyst for efficient photocatalysis. However, when the molar ration proportion of PANI exceeded 1:40, the photodegradation rate was decreased but still larger than that of origin MS-TiO_2. The results mentioned above showed that the uptake amount of PANI played a vital role on the photocatalytic process. It can be confirmed that the best performance of PANI/MS-TiO_2 resulted from the lowest recombination of photoinduced electron-hole pairs and the fastest transportation of the photogenerated charges.

Taken the practical application into consideration, it is necessary to evaluate the longevity and stability of PANI/MS-TiO_2. In the recycling experiments, the best performance photocatalyst (PANI/MS-TiO_2 (1:40)) was chosen as the target photocatalyst for the degradation of RhB and MB under visible light irradiation (Fig. 12). It is found that the removal efficiency of both of RhB and MB kept as high as 90% after five consecutive recycles. In order to ensure the accuracy of the experiment, when the former experiment was finished, the photocatalyst were washed with water thoroughly to remove the unreacted RhB or MB. The unique mesoporous single crystal and microsphere structure of MS-TiO_2 brought about the highly stable photocatalytic activity of PANI/MS-TiO_2 photocatalysts. The high photocatalytic activity and stability might make the practical application become reality.

3.9. Photocatalytic degradation mechanism

To detect the main oxidative species formed in the PANI/MS-TiO_2 composite and to understand the mechanism of the photocatalysis process, a series of radical and holes trapping experiments were conducted by adding different kinds of active species scavengers in the photocatalysis degradation system. Generally, three typical chemical reagents, TEOA serving as hole scavenger (h^+), IPA serving as hydroxyl radical scavenger ($^\bullet OH$) and BQ serving as superoxide radical scavenger ($^\bullet O_2^-$), were added in the RhB degradation over PANI/MS-TiO_2 (1:40) under visible light irradiation, respectively. As shown in Fig. 13, when TEOA was added into the photocatalytic system, the photocatalytic degradation efficiency of RhB decreased dramatically, suggesting that h^+ served as the dominant active species which accounted for the degradation of dye pollutants under visible light irradiation. Besides, the BQ also inhibited the photocatalytic activity of PANI/MS-TiO_2 (1:40) greatly, indicating that $^\bullet O_2^-$ also had great influence on the visible light photodegradation process. However, the photodegradation efficiency of RhB just experienced a very little reduction when IPA was added, which means that effect of hydroxyl radical was weak. So, according to the results mentioned above, it is clear to notice

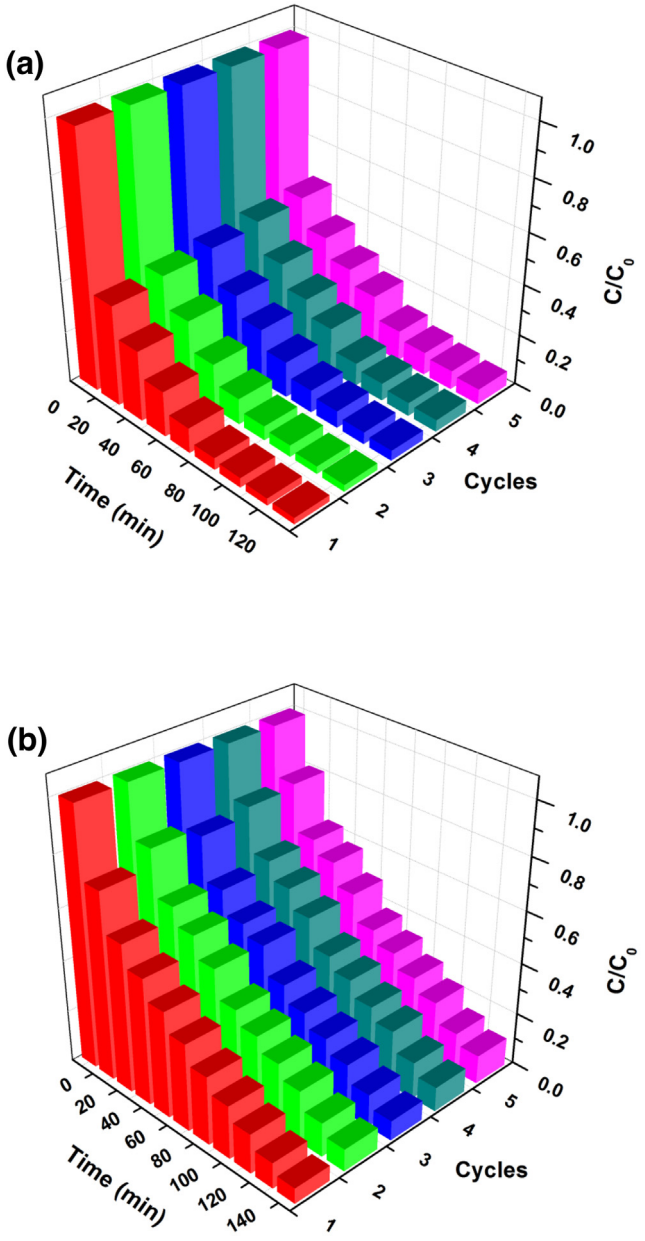

Fig. 12. Recycling runs of the PANI/MS-TiO_2 (1:40) for the degradation of (a) RhB and (b) MB under visible light irradiation.

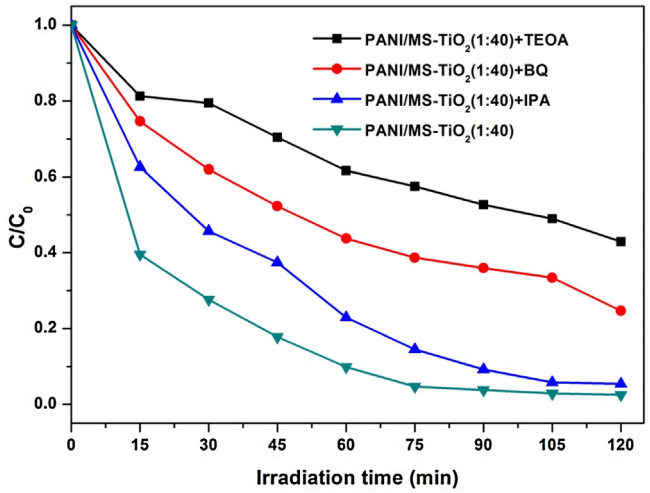

Fig. 13. Trapping experiment of active species during the photocatalytic degradation of RhB over different PANI/MS-TiO_2 under visible light (λ > 400 nm) irradiation.

that both photogenerated superoxide radical and holes, especially holes, were responsible for the photodegradation of RhB.

As we know, some properties, such as light harvest efficiency, interfacial reaction process, and the transportation efficiency of the photogenerated charges, jointly determined the overall photocatalytic activity of the photocatalyst. For the as prepared PANI/MS-TiO_2 photocatalyst, it presented remarkable photocatalytic activity on the degradation of RhB or MB under visible light irradiation. The reasons can be explained in the following two aspects: on one hand, the mesoporous single crystal and microsphere structure of TiO_2 could facilitate the optical path length and increase the transmission of light waves among the photocatalyst by scattering of visible light and multiple reflections within the interior space; on the other hand, the large specific surface area of the MS-TiO_2 can increase the uptake amount of the PANI, which could promote the visible light harvest efficiency. Meanwhile, the single crystal structure could promote the photogenerated charge transfer and separation, and the high specific surface area could provide more active sites for the photodegradation process. All the reasons mentioned above contributed to the high photodegradation efficiency of PANI/MS-TiO_2 photocatalyst.

To more clearly present the process of photodegradation, the photodegradation mechanism of organic pollutant over PANI/MS-TiO_2 photocatalyst is proposed in Scheme 2. According to the results of photodegradation and the radical experiments, the photodegradation mechanics under visible light (λ > 400 nm) can be explained as follows: first of all, under visible light irradiation, PANI can be induced and produce π-π* transition, and then the induced excited-state electrons are separated and transported from the π-orbital to π*-orbital; it is well known that the d-orbital in conductor band of TiO_2 matched well with the π*-orbital of PANI in energy level, which could lead to synergistic effect; due to the synergistic effect, the induced and excited-state electrons could facilely transfer to the d-orbital or conductor band of TiO_2 and eventually transfer to the surface of the TiO_2 to react with the dissolved oxygen molecules to yield superoxide ($^{\bullet}O_2^-$), and subsequently the organic pollutants would be oxidized by the generated holes and radicals. As mentioned above, the generated process of the main reactive species and the major reactions occurred in the photodegradation of organic pollutants can be ascribed as follows.

$$\text{PANI/TiO}_2 + h\nu \rightarrow \text{PANI/TiO}_2(h_{VB}^{+}) + e_{CB}^{-} \quad (2)$$

$$e_{CB}^{-} + O_2 \rightarrow {}^{\bullet}O_2^{-} \quad (3)$$

$$\text{PANI/TiO}_2(h_{VB}^{+}) \rightarrow \text{PANI/TiO}_2 + h_{VB}^{+} \quad (4)$$

$$(5)\ h_{VB}^{+} + \text{RhB/MB} \rightarrow \text{degradationproducts}$$

$$^{\bullet}O_2^{-} + \text{RhB/MB} \rightarrow \text{degradationproducts} \quad (6)$$

4. Conclusions

In summary, an efficient visible light responsive photocatalyst has been prepared successfully by employing mesoporous single crystal TiO_2 microsphere to the PANI/MS-TiO_2 in this study. Under the optimal conditions (PANI/MS-TiO_2 (1:40)), 99.8% of RhB (99.5% of MB) can be removed in 120 min (in 150 min) under visible light irradiation. In the process of photocatalytic degradation, the PANI/MS-TiO_2 presented better performance than pristine MS-TiO_2 under visible light irradiation. This phenomenon can be attributed to the large load amount of PANI molecular, which

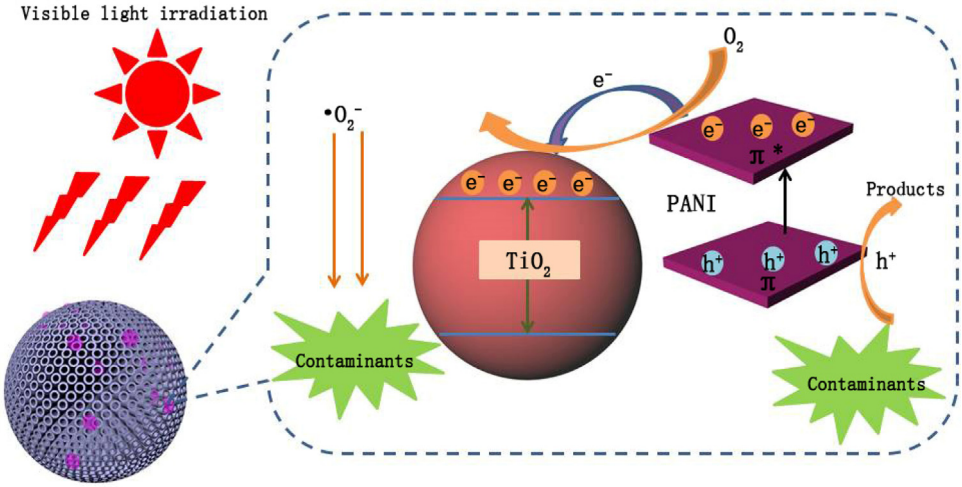

Scheme 2. Diagram of the photocatalytic reaction process on PANI/MS-TiO_2 photocatalyst.

increases the visible light absorption ability of the PANI/MS-TiO_2. Besides, the single crystal structure of MS-TiO_2 and the synergistic effect between PANI and TiO_2 can promote the separation efficiency of photogenerated charges, which also plays a role in improving the photocatalytic performance. We believe that this work could provide a new insight into the preparation of high efficient photocatalyst by using a facial surface modification method and make it possible for realistic application for the treatment of dye wastewater.

Acknowledgments

The study was financially supported by the National Program for Support of Top–Notch Young Professionals of China (2012), Projects 51579096, 51222805, 51521006 and 51508175 supported by National Natural Science Foundation of China, the Program for New Century Excellent Talents in University from the Ministry of Education of China (NCET–11–0129), the Hunan Province Innovation Foundation for Postgraduate (CX2015B095).

References

[1] M.H. Cao, P.F. Wang, Y.H. Ao, C. Wang, J. Hou, J. Qian, Photocatalytic degradation of tetrabromobisphenol A by a magnetically separable graphene–TiO_2 composite photocatalyst: mechanism and intermediates analysis, Chem. Eng. J. 264 (2015) 113–124.
[2] J.G. Yu, X.X. Yu, Hydrothermal synthesis and photocatalytic activity of zinc oxide hollow spheres, Environ. Sci. Technol. 42 (2008) 4902–4907.
[3] M.J. Chen, S.L. Lo, Y.C. Lee, C.C. Huang, Photocatalytic decomposition of perfluorooctanoic acid by transition-metal modified titanium dioxide, J. Hazard. Mater. 288 (2015) 168–175.
[4] Z.X. Li, Y. Shen, C. Yang, Y.C. Lei, Y.H. Guan, Y.H. Lin, D.B. Liu, C.W. Nan, Significant enhancement in the visible light photocatalytic properties of $BiFeO_3$–graphene nanohybrids, J. Mater. Chem. A 1 (2013) 823–829.
[5] S. Sakthivel, M.V. Shankar, M. Palanichamy, B. Arabindoo, D.W. Bahnemann, V. Murugesan, Enhancement of photocatalytic activity by metal deposition: characterisation and photonic efficiency of Pt, Au and Pd deposited on TiO_2 catalyst, Water Res. 38 (2004) 3001–3008.
[6] L. Tang, J.J. Wang, G.M. Zeng, Y.N. Liu, Y.C. Deng, Y.Y. Zhou, J. Tang, J.J. Wang, Z. Guo, Enhanced photocatalytic degradation of norfloxacin in aqueous Bi_2WO_6 dispersions containing nonionic surfactant under visible light irradiation, J. Hazard. Mater. 306 (2015) 295–304.
[7] F. Chen, Q. Yang, C.G. Niu, X.M. Li, C. Zhang, G.M. Zeng, Plasmonic photocatalyst Ag@AgCl/$ZnSn(OH)_6$: synthesis, characterization and enhanced visible-light photocatalytic activity in the decomposition of dyes and phenol, RSC Adv. 5 (2015) 63152–63164.
[8] J. Liu, Q. Zhang, J. Yang, H. Ma, M.O. Tade, S. Wang, J. Liu, Facile synthesis of carbon-doped mesoporous anatase TiO_2 for the enhanced visible-light driven photocatalysis, Chem. Commun. 50 (2014) 13971–13974.
[9] X.B. Chen, S.M. Mao, Titanium dioxide nanomaterials: synthesis, properties, modifications, and applications, Chem. Rev 107 (2007) 2891–2959.
[10] M. Mohamed, M.S. Al-Sharif, Visible light assisted reduction of 4-nitrophenol to 4-aminophenol on Ag/TiO_2 photocatalysts synthesized by hybrid templates, Appl. Catal. B Environ. 142-143 (2013) 432–441.
[11] Y.F. Yang, Z. Ma, L.D. Xu, H.F. Wang, N. Fu, Preparation of reduced graphene oxide/meso-TiO_2/AuNPs ternary composites and their visible-light-induced photocatalytic degradation n of methylene blue, Appl. Surf. Sci. 369 (2016) 576–583.
[12] J.F. Zhu, W. Zheng, B. He, J.L. Zhang, M. Anpo, Characterization of Fe–TiO_2 photocatalysts synthesized by hydrothermal method and their photocatalytic reactivity for photodegradation of XRG dye diluted in water, J. Mol. Catal. A Chem. 216 (2004) 35–43.
[13] W.D. Wang, P. Serp, P. Kalck, J.L. Faria, Visible light photodegradation of phenol on MWNT-TiO_2 composite catalysts prepared by a modified sol–gel method, J. Mol. Catal. A Chem. 235 (2005) 194–199.
[14] W. Zhou, Z. Yin, Y. Du, X. Huang, Z. Zeng, Z. Fan, H. Liu, J. Wang, H. Zhang, Synthesis of few-layer MoS_2 nanosheet-coated TiO_2 nanobelt heterostructures for enhanced photocatalytic activities, Small 9 (2013) 140–147.
[15] J. Tian, P. Hao, N. Wei, H.Z. Cui, H. Liu, 3D Bi_2MoO_6 Nanosheet/TiO_2 nanobelt heterostructure: enhanced photocatalytic activities and photoelectochemistry performance, ACS Catal. 5 (2015) 4530–4536.
[16] L. Tang, Y.C. Deng, G.M. Zeng, W. Hu, J.J. Wang, Y.Y. Zhou, J.J. Wang, J. Tang, W. Fang, CdS/Cu_2S co-sensitized TiO_2 branched nanorod arrays of enhanced photoelectrochemical properties by forming nanoscale heterostructure, J. Alloy. Compd. 662 (2016) 516–527.
[17] B. Sun, G.W. Zhou, T.T. Gao, H.J. Zhang, H.H. Yu, NiO nanosheet/TiO_2 nanorod-constructed p–n heterostructures for improved photocatalytic activity, Appl. Surf. Sci. 364 (2016) 322–331.
[18] X.J. Zou, Y.Y. Dong, X.D. Zhang, Y.B. Cui, Synthesize and characterize of Ag_3VO_4/TiO_2 nanorods photocatalysts and its photocatalytic activity under visible light irradiation, Appl. Surf. Sci. 366 (2016) 173–180.
[19] F. Deng, L. Min, X. Luo, S. Wu, S. Luo, Visible-light photocatalytic degradation performances and thermal stability due to the synergetic effect of TiO_2 with conductive copolymers of polyaniline and polypyrrole, Nanoscale 5 (2013) 8703–8710.
[20] H.C. Liang, X.Z. Li, Visible-induced photocatalytic reactivity of polymer–sensitized titania nanotube films, Appl. Catal. B Environ. 86 (2009) 8–17.
[21] D.S. Wang, J. Zhang, Q.Z. Luo, X.Y. Li, Y.D. Duan, J. An, Characterization and photocatalytic activity of poly(3-hexylthiophene)-modified TiO_2 for degradation of methyl orange under visible light, J. Hazard. Mater. 169 (2009) 546–550.
[22] H. Zhang, R.L. Zong, J.C. Zhao, Y.F. Zhu, Dramatic visible photocatalytic degradation performances due to synergetic effect of TiO_2 with PANI, Environ. Sci. Technol. 42 (2008) 3803–3807.
[23] M.A. Salem, A.F. Al-Ghonemiy, A.B. Zaki, Photocatalytic degradation of allura red and quinoline yellow with Polyaniline/TiO_2 nanocomposite, Appl. Catal. B Environ. 91 (2009) 59–66.
[24] B. Tian, X. Liu, B. Tu, C. Yu, J. Fan, L. Wang, S. Xie, G.D. Stucky, D. Zhao, Self-adjusted synthesis of ordered stable mesoporous minerals by acid-base pairs, Nat. Mater. 2 (2003) 159–163.
[25] E.J.W. Crossland, N. Noel, V. Sivaram, T. Leijtens, J.A. Alexander-Webber, H.J. Snaith, Mesoporous TiO_2 single crystals delivering enhanced mobility and optoelectronic device performance, Nature 495 (2013) 215–219.
[26] L. Tang, S. Zhang, G.M. Zeng, Y. Zhang, G.D. Yang, J. Chen, J.J. Wang, J.J. Wang, Y.Y. Zhou, Y.C. Deng, Rapid adsorption of 2,4-dichlorophenoxyacetic acid by iron oxide nanoparticles-doped carboxylic ordered mesoporous carbon, J. Colloid Interface Sci. 445 (2015) 1–8.

[27] Y. Zhou, L. Tang, G. Zeng, J. Chen, Y. Cai, Y. Zhang, G. Yang, Y. Liu, C. Zhang, W. Tang, Mesoporous carbon nitride based biosensor for highly sensitive and selective analysis of phenol and catechol in compost bioremediation, Biosens. Bioelectron. 61 (2014) 519–525.
[28] L. Tang, Y. Fang, Y. Pang, G. Zeng, J. Wang, Y. Zhou, Y. Deng, G. Yang, Y. Cai, J. Chen, Synergistic adsorption and reduction of hexavalent chromium using highly uniform polyaniline–magnetic mesoporous silica composite, Chem. Eng. J. 254 (2014) 302–312.
[29] L. Tang, G.D. Yang, G.M. Zeng, Y. Cai, S.S. Li, Y.Y. Zhou, Y. Pang, Y.Y. Liu, Y. Zhang, B. Luna, Synergistic effect of iron doped ordered mesoporous carbon on adsorption-coupled reduction of hexavalent chromium and the relative mechanism study, Chem. Eng. J. 239 (2014) 114–122.
[30] G.Z. Liao, S. Chen, X. Quan, Y.B. Zhang, H.M. Zhao, Remarkable improvement of visible light photocatalysis with PANI modified core–shell mesoporous TiO_2 microspheres, Appl. Catal. B Environ. 102 (2011) 126–131.
[31] Y. Liu, R.C. Che, G. Chen, J.W. Fan, Z.K. Sun, Z.K. Wu, M.H. Wang, B. Li, J. Wei, Y. Wei, G. Wang, G.Z. Guan, A.A. Elzatahry, A.A. Bagabas, A.M. Al-Enizi, Y.H. Deng, H.S. Peng, D.Y. Zhao, Radially oriented mesoporous TiO_2 microspheres with single-crystal–like anatase walls for high-efficiency optoelectronic devices, Sci. Adv. (2015).
[32] D. Hidalgo, S. Bocchini, M. Fontana, G. Saracco, S. Hernandez, Green and low-cost synthesis of PANI-TiO_2 nanocomposite mesoporous films for photoelectrochemical water splitting, RSC Adv. 5 (2015) 49429–49438.
[33] X.Y. Li, D.S. Wang, G.X. Cheng, Q.Z. Luo, J. An, Y.H. Wang, A.A. Bagabas, Preparation of polyaniline-modified TiO_2 nanoparticles and their photocatalytic activity under visible light illumination, Appl. Catal. B Environ. 81 (2008) 267–273.
[34] N. Guo, Y.M. Liang, S. Lan, L. Liu, J.J. Zhang, G.J. Ji, S.C. Gan, Microscale hierarchical three-dimensional flowerlike TiO_2/PANI composite: synthesis, characterization, and its remarkable photocatalytic activity on organic dyes under UV-light and sunlight irradiation, J. Phys. Chem. C 118 (2014) 18343–18355.
[35] L.A. Gu, J.Y. Wang, R. Qi, X.Y. Wang, P. Xu, X.J. Han, A novel incorporating style of polyaniline/TiO_2 composites as effective visible photocatalysts, J. Mol. Catal. A Chem. 357 (2012) 19–25.
[36] Q.Z. Luo, L.L. Bao, D.S. Wang, X.Y. Li, J. An, Preparation and strongly enhanced visible light photocatalytic activity of TiO_2 nanoparticles modified by conjugated derivatives of polyisoprene, J. Phys. Chem. C 116 (2012) 25806–25815.
[37] P. Xiong, L.J. Wang, X.Q. Sun, B.H. Xu, X. Wang, Ternary titania–cobalt Ferrite–polyaniline nanocomposite: a magnetically recyclable hybrid for adsorption and photodegradation of dyes under visible light, Ind. Eng. Chem. Res. 52 (2013) 10105–10113.
[38] X.F. Hu, T. Mohamood, W.H. Ma, C.C. Chen, J.C. Zhao, Oxidative decomposition of rhodamine b dye in the presence of VO^{2+} and/or Pt(IV) under visible light irradiation: N-deethylation, chromophore cleavage, and mineralization, J. Phys. Chem. B 110 (2006) 26012–26018.
[39] J. Zhuang, W. Dai, Q. Tian, Z. Li, L. Xie, J. Wang, P. Liu, X. Shi, D. Wang, Photocatalytic degradation of RhB over TiO_2 bilayer films: effect of defects and their location, Langmuir: ACS J. Surf. Colloids 26 (2010) 9686–9694.
[40] T.Y. Zhang, T. Oyamaa, A. Aoshima, H. Hidaka, J.C. Zhao, N. Serpone, PhotooxidativeN-demethylation of methylene blue in aqueous TiO_2 dispersions under UV irradiation, J. Photochem. Photobiol. A 140 (2001) 163–172.
[41] C.B. Liu, D.S. Meng, Y. Li, L.L. Wang, Y.T. Liu, S.L. Luo, Hierarchical architectures of ZnS–In2S_3 solid solution onto TiO_2 nanofibers with high visible-light photocatalytic activity, J. Alloys Compd. 624 (2015) 44–52.
[42] S. Yamazaki, N. Nakamura, Photocatalytic reactivity of transparent titania sols prepared by peptization of titanium tetraisopropoxide, J. Photoch. Photobio. A 193 (2008) 65–71.